communications biology

Article

https://doi.org/10.1038/s42003-024-06941-9

Coordinated NREM sleep oscillations among hippocampal subfields modulate synaptic plasticity in humans

Check for updates

Zhipeng Li[1,2,17], Jing Wang[3,17], Chongyang Tang[4,17], Peng Wang[5], Peng Ren[6], Siyang Li[7], Liye Yi[8], Qiuyi Liu[1,2], Lili Sun[1,2], Kaizhou Li[1,2], Wencai Ding[9], Hongbo Bao[10,11], Lifen Yao[12], Meng Na[13] ✉, Guoming Luan[4,14] ✉ & Xia Liang[1,2,15,16] ✉

The integration of hippocampal oscillations during non-rapid eye movement (NREM) sleep is crucial for memory consolidation. However, how cardinal sleep oscillations bind across various subfields of the human hippocampus to promote information transfer and synaptic plasticity remains unclear. Using human intracranial recordings from 25 epilepsy patients, we find that hippocampal subfields, including DG/CA3, CA1, and SUB, all exhibit significant delta and spindle power during NREM sleep. The DG/CA3 displays strong coupling between delta and ripple oscillations with all the other hippocampal subfields. In contrast, the regions of CA1 and SUB exhibit more precise coordination, characterized by event-level triple coupling between delta, spindle, and ripple oscillations. Furthermore, we demonstrate that the synaptic plasticity within the hippocampal circuit, as indexed by delta-wave slope, is linearly modulated by spindle power. In contrast, ripples act as a binary switch that triggers a sudden increase in delta-wave slope. Overall, these results suggest that different subfields of the hippocampus regulate one another through diverse layers of sleep oscillation synchronization, collectively facilitating information processing and synaptic plasticity during NREM sleep.

The endogenously generated brain oscillations during NREM sleep play a crucial role in information processing for memory consolidation[1–5]. Specifically, the high frequency ripple events (~80–100 Hz in humans) generated by the hippocampus is associated with reactivation of recently learned information[6–8]. The occurrences of hippocampal ripples are tightly coupled with cortical slow oscillations (SO; <1.25 Hz), delta waves (1–4 Hz) and sleep spindles (12–16 Hz)[9–13]. The systematic couplings of these brain oscillations suggest intricately timed information transfer between the underlying hippocampal and cortical circuits, forming the electrophysiological underpinnings for the memory function of NREM sleep[14–19].

Recent studies have unveiled the presence of multiple layers of coupling among the NREM sleep rhythms within the hippocampus, highlighting their role in facilitating information transfer not only between the hippocampus and cortex but also within the hippocampus itself[20–26]. In fact, the complexity of hippocampal function extends beyond the coexistence of these diverse brain waveforms. The hippocampal formation is a complex structure composed of the dentate gyrus (DG), the hippocampal proper (including the CA subfields),

[1]School of Life Science and Technology, HIT Faculty of Life Science and Medicine, Harbin Institute of Technology, Harbin, 150001, China. [2]Laboratory for Space Environment and Physical Sciences, Harbin Institute of Technology, Harbin, 150001, China. [3]Department of Neurology, SanBo Brain Hospital, Capital Medical University, Beijing, 100093, China. [4]Department of Neurosurgery, SanBo Brain Hospital, Capital Medical University, Beijing, 100093, China. [5]Institute of Psychology, University of Greifswald, Greifswald, Germany. [6]Institute of Science and Technology for Brain-Inspired Intelligence and Department of Neurology, Huashan Hospital, Fudan University, Shanghai, China. [7]Zhejiang Lab, Hangzhou, Zhejiang, 311100, China. [8]The Second Affiliated Hospital of Harbin Medical University, Harbin, China. [9]Department of Neurology, The Second Affiliated Hospital of Wannan Medical College, Wuhu, China. [10]Department of Neurosurgery, Harbin Medical University Cancer Hospital, 150081 Harbin, China. [11]Department of Neurosurgery, BeijingTiantan Hospital, Capital Medical University, 100070 Beijing, China. [12]Department of Neurology, The First Affiliated Hospital of Harbin Medical University, Harbin, 150001, China. [13]Department of Neurosurgery, The First Affiliated Hospital of Harbin Medical University, Harbin, 150001, China. [14]Center of Epilepsy, Beijing Institute for Brain Disorders, Beijing, 100093, China. [15]Frontiers Science Center for Matter Behave in Space Environment, Harbin Institute of Technology, Harbin, 150001, China. [16]Research Center for Social Computing and Information Retrieval, Harbin Institute of Technology, Harbin, China. [17]These authors contributed equally: Zhipeng Li, Jing Wang, Chongyang Tang. ✉e-mail: nameng2001@hotmail.com; luangm@ccmu.edu.cn; xia.liang@hit.edu.cn

and the subiculum (SUB). These hippocampal subfields are extensively interconnected. For instance, along the most well-characterized tri-synaptic pathway, which serves as the primary intra-hippocampal route for information flow, information traverses from the DG to CA3 and subsequently to CA1[27–30]. The outputs of CA1 are then projected to the SUB, which serves as a relay station for transmitting information to diverse cortical and subcortical regions[27,31,32]. Given that oscillatory coupling has been established as a critical mechanism for interregional information transmission in the brain[18,33,34], we hypothesize that information coordination within the hippocampal circuit can be achieved through tight coupling among the cardinal NREM oscillations between different hippocampal subfields. Moreover, increasing evidence has suggested that each hippocampal subfield plays a unique role in processing information essential for memory formation and consolidation[27,35–37]. Thus, we hypothesize further that different hippocampal subfields may exhibit distinct profiles of sleep oscillation coupling during NREM sleep.

Sleep is accompanied by a balance of global synaptic downscaling and local synaptic upscaling[38–43]. As suggested by the synaptic homeostasis hypothesis, the global synaptic downscaling is regulated by the homeostasis process and primarily takes place during rapid eye movement (REM) sleep[44]. On the other hand, selected synaptic upscaling is more linked to NREM sleep, which helps preserve learning-related information[18]. The process of synaptic homeostasis is reflected in delta wave activity[45,46], which has been suggested to be generated by near-synchronous oscillations of large groups of neurons at the cellular level[47,48]. The slope of delta waves, which reflects their amplitude and steepness, is closely tied to the firing synchronicity and efficiency of neuronal interactions[45,46]. A steeper slope corresponds to stronger synaptic connections, typically observed after learning and synaptic potentiation[2,49,50]. As synaptic downscaling occurs during sleep, there is a corresponding reduction in the slow wave slope, mirroring the decrease in synaptic strength and density[51]. While the delta wave activity has been considered an indirect but effective marker of synaptic plasticity and homeostasis, the other sleep events including spindle and ripple have been suggested to provide crucial time windows for synaptic reshaping[9,52–56]. However, there is a lack of research investigating the specific impact of hippocampal spindle and ripple oscillations on synaptic potentiation during NREM sleep. We thus hypothesize that hippocampal spindles and ripples may have distinct roles in regulating synaptic potentiation, which could be reflected in their associations with changes in delta-wave slope during NREM sleep.

In this study, we conducted intracranial EEG (iEEG) recordings in 25 epilepsy patients during NREM sleep, focusing on three hippocampal subfields: the DG/CA3, CA1, and SUB. Our findings revealed that while the DG/CA3 displayed strong coupling between delta and ripple oscillation with all hippocampal subfields, the CA1 and SUB showed a more precise coordination involving triple synchronization between delta, spindle, and ripple events. Furthermore, we showed that the synaptic plasticity within the hippocampal circuit, as indexed by delta-wave slope, are linearly modulated by the spindle power. In contrast, ripples appeared to act as a binary switch that trigger sudden increase in delta-wave slope.

Results

Spectral profiles of different hippocampal subfields during NREM sleep

Using preoperative structural MRI and postoperative CT scans, we identified iEEG recording electrodes[57] located within the three hippocampal subfields, namely the DG/CA3, CA1 and SUB, in each participant. Due to the lack of clinical sleep hypnograms, patient monitoring videos, scalp EEG, and electrooculograms, we selected NREM sleep (including N2 and N3 stages) based on *neocortical* iEEG signals by identifying prolonged elevations in low delta band (<2 Hz) activity amplitude and corresponding declines in high-gamma (HG; 70–190 Hz) and initially high but gradually decreasing spindle band amplitudes[58,59] (Fig. 1a). This procedure obtained a total of 1548 min of NREM sleep across all subjects. Please refer to Supplementary Table 1 for details.

After identifying the hippocampal electrodes, we analyzed the spectral characteristics of the three hippocampal subfields during NREM sleep using Welch's method[60]. The spectral results revealed strong power in the delta and spindle frequency band for all hippocampal subfields during NREM sleep (Fig. 1b, c). This is consistent with earlier studies that have reported high delta and spindle activity in the hippocampus during NREM[23,60,61].When comparing the spectral power between the three subfields, we found that the DG/CA3 showed an overall trend of higher power than the CA1, and SUB, with certain frequency bands showing significant differences (cluster-based permutation test, $p < 0.001$; DG/CA3 > CA1: 10–11 Hz; DG/CA3 > SUB: 27–30 Hz; Fig. 1b and Supplementary Fig. 2b). To compare the dominant frequencies within each hippocampal subfield, we normalized the spectrum for each subfield and observed that the spindle band of SUB was significantly higher than that of DG/CA3 (cluster-based permutation test, $p < 0.001$; Fig. 1b inset and Supplementary Fig. 2c). We also showed scatter plots of the spectral mean in 0–200 Hz (Supplementary Fig. 2d), as well as 10–11 Hz, 12–15 Hz, and 27–30 Hz (these bands showed significant differences; Supplementary Fig. 2e–g).

High delta-ripple coupling within the DG/CA3

Next, we employed Mean Vector Length (MLV)[60,62] method to explore the cross-frequency phase-amplitude coupling (PAC) within each of the three hippocampal subfields. The results showed that the DG/CA3 exhibited significant delta-ripple coupling ($p < 0.05$, corrected; Fig. 2a). While the high-frequency range of coupling extends beyond the ripple range and can include the high gamma and even higher frequencies, we will refer to it as "ripple" for convenience since it constitutes the core coupling band. The DG/CA3 also exhibited significant delta-theta coupling (1/3–3/8 Hz; $p < 0.05$, corrected; Fig. 2a). The CA1 and SUB, on the other hand, did not exhibit any significant phase-amplitude coupling (Fig. 2a).

The high delta-ripple coupling within the hippocampus may reflect sharp wave-ripple (SWR) complexes which is composed of ripples co-occurring with large-amplitude slow sharp waves[63–65]. Therefore, we extracted ripple events from each hippocampal subfield (±0.5 s; mean ± SEM; Fig. 2b) and observed that these ripple events were indeed superimposed on sharp waves (Fig. 2c), providing evidence supporting that the delta-ripple coupling might indicate the existence of SWR complexes. We note that the low-frequency span of DG/CA3 extended up to 8 Hz. This is consistent with the characteristics of sharp waves in SWR, as previous research has shown that the frequency range of sharp waves in SWR can reach up to 10 Hz[60]. Note that although only the DG/CA3 exhibited delta-ripple coupling in the PAC analyses at the band level, the CA1 and the SUB also displayed SWR at the event level. This suggests that the delta-ripple coupling in the CA1 and SUB might be more intricate which only manifests within narrow time windows associated with ripple events. We further explored the coupling phase of ripple to delta wave. We calculated the probability of delta phase corresponding to the maximum ripple. We found that ripples of the DG/CA3 and CA1 coupled with delta wave at a phase around 0–90°, while the SUB exhibited delta-ripple coupling around 180° of delta wave (*Rayleigh*-test, Bonferroni correction, $p < 0.001$; DG/CA3: 65.8°; CA1: 24.8°; SUB: 169.3°; Fig. 2d). This could potentially be attributed to the distinct structural and functional characteristics of the SUB in comparison to the other hippocampal subfields[27,66].

Delta-spindle-ripple coupling in CA1 and SUB, but not in DG/CA3

In the above PAC analysis, we did not observe any delta-spindle or spindle-ripple coupling, which are known to be highly relevant to the hippocampus during NREM sleep. Previous studies on hippocampal delta-spindle and spindle-ripple coupling have primarily relied on event-based analyses[21,60]. Hence, we proceeded to explore whether the hippocampal subfields exhibit delta-spindle and spindle-ripple coupling using spindle event-locked PAC analysis.

We extracted spindle events from the three subfields (±1.5 s; mean ± SEM; Fig. 3a), and computed delta-spindle coupling from −1 s to +1 s and spindle-ripple couplings from −0.25 s to +0.25 s around the spindle center. We found that delta-spindle coupling was present in all three hippocampal subfields (*V*-test, Bonferroni correction, $p < 0.05$; significant coupling phases: DG/CA3: 40 to 60°; CA1: −180 to −80°; SUB: 0 to 120°; Fig. 3b). Spindle-ripple coupling, on the other hand, only appeared within the CA1 and SUB (*V*-

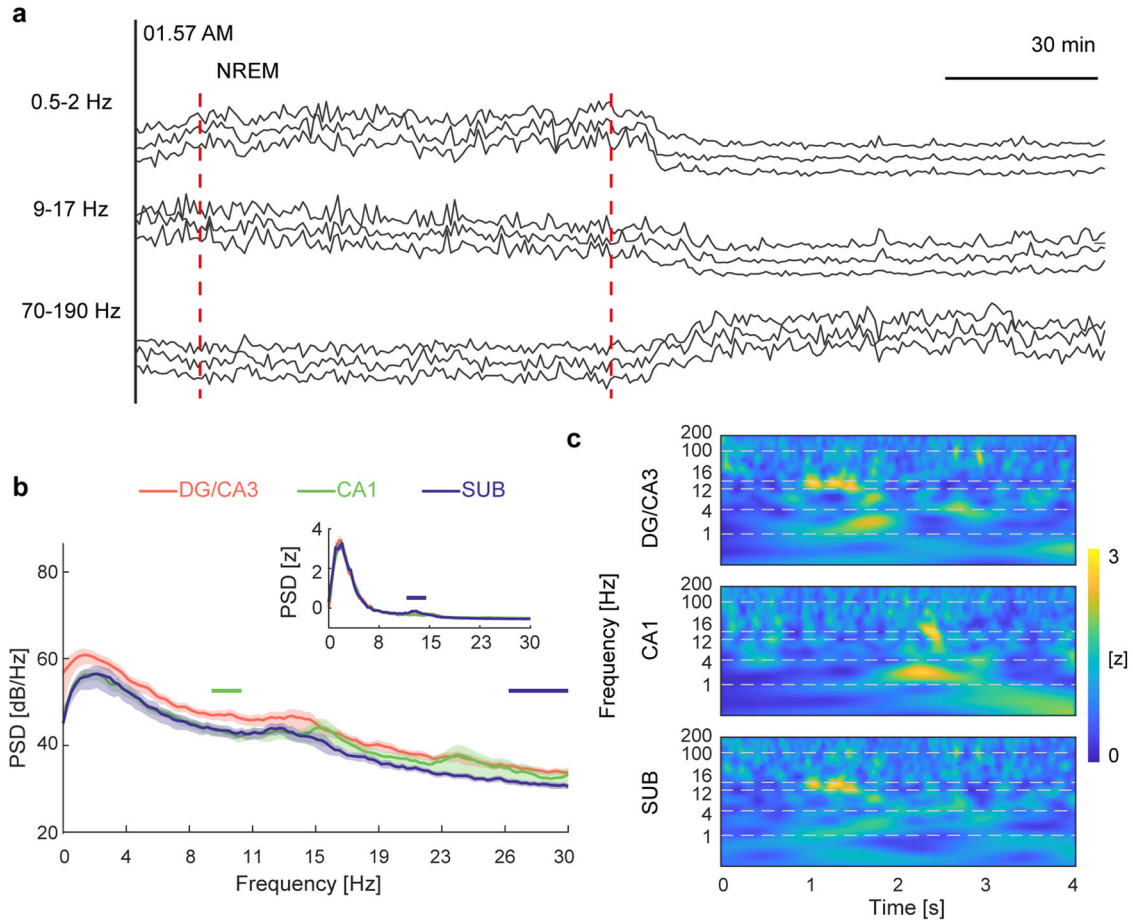

Fig. 1 | Identification of NREM sleep, and spectra in DG/CA3, CA1, and SUB. **a** Identification of NREM sleep (stages N2 and N3) using spectral power. The Hilbert analytic amplitudes of sleep LFP in the spindle (9–17 Hz), low delta (0.5–2 Hz), and high gamma (70–190 Hz) bands were calculated to identify NREM (between the two vertical red lines is the NREM state). All error bars indicate the mean ± SEM. **b** The spectra showed strong power in the delta and spindle band for all hippocampal subfields. Comparisons of the spectra between the three subfields revealed that the DG/CA3 had higher power than CA1 and SUB in specific bands (cluster-based permutation test, $p < 0.001$; green represents DG/CA3 > CA1: 10–11 Hz; purple represents DG/CA3 > SUB: 27–30 Hz). Inset: Comparisons of the normalized spectra between the three subfields (cluster-based permutation test, $p < 0.001$; purple represents SUB > DG/CA3: spindle band, 12–15 Hz). **c** Shown were 4 s *z*-scored spectrograms for three subfields of artifact-free data from a single patient. Prominent frequencies were delta bands, spindle bands and high frequency bursts (around 100 Hz). All error bars indicate the mean ± SEM.

test, Bonferroni correction, $p < 0.05$; CA1: 140 to 200°; SUB: −40 to 40°; Fig. 3c). The presence of both delta-spindle coupling and spindle-ripple coupling (Fig. 3b–d) indicates triple coordination between the delta, spindle and ripple activity in the CA1 and SUB. Therefore, we sought to examine whether delta-spindle coupling would modulate ripple activity in the CA1 and SUB. To this end, we computed the ripple power in relation to the delta-spindle coupling phase (Fig. 3e). Our analysis revealed a significant correlation between ripple power and delta-spindle coupling phase in CA1 ($r = 0.56$, $p = 0.0037$, the highest ripple power was observed around −145°), while no significant correlation was observed in the SUB region.

Previous studies have shown that there is an event-based coupling of SO-spindle in the hippocampus during NREM sleep[21]. We thus analyzed the SO-spindle coupling in each hippocampal subfield here. To avoid overlap with the delta frequency, the frequency range of SO here is limited to 0.2–1 Hz. Unlike the observed delta-spindle-ripple coupling in the CA1 field, we found that there was no substantial coupling between SO and spindles within the CA1 subfield (Supplementary Fig. 3a). In addition, no other subfield was observed to show any modulation of SO–spindle phase on ripple power (Supplementary Fig. 3b).

Inter-regional coupling between hippocampal subfields

We next sought to investigate how delta, spindle and ripple oscillations are coupled between different hippocampal subfields during NREM sleep. Band-based PAC analysis revealed that the DG/CA3 exhibited significant coupling with the CA1 and SUB, with the frequency range primarily concentrated in the delta-ripple ($p < 0.05$, corrected; Fig. 4a). There was no significant PAC between the CA1 and SUB. Nevertheless, when analyzing the spindle event-locked phase-amplitude coupling, we found significant delta-spindle (*V*-test, Bonferroni correction, $p < 0.05$; CA1-SUB: −180 to −60°; SUB-CA1: 20 to 120°; Fig. 4b, c) and spindle-ripple (*V*-test, Bonferroni correction, $p < 0.05$; CA1-SUB: −60 to 40°; SUB-CA1: 120 to 240°; Fig. 4b, c) couplings between the CA1 and SUB. The delta-spindle-ripple couplings between the CA1 and SUB were also illustrated in raw traces in Fig. 4d. These inter-regional coupling results resembled those from the intra-regional coupling analyses, with band-based cross-frequency coupling was mainly observed in the DG/CA3 subfield, while event-based coupling was predominantly presented between the CA1 and SUB. Spindle event-based coupling between DG/CA3 and CA1, and between DG/CA3 and SUB did not show significant couplings, either for delta-spindle or spindle-ripple (Supplementary Fig. 4).

Differential regulation of delta slope by hippocampal spindle and ripple events

In a final step, we proceeded to explore the role of spindle and ripple events in regulating synaptic plasticity in different hippocampal subfields during NREM sleep. Prior studies have demonstrated that the plastic changes in net

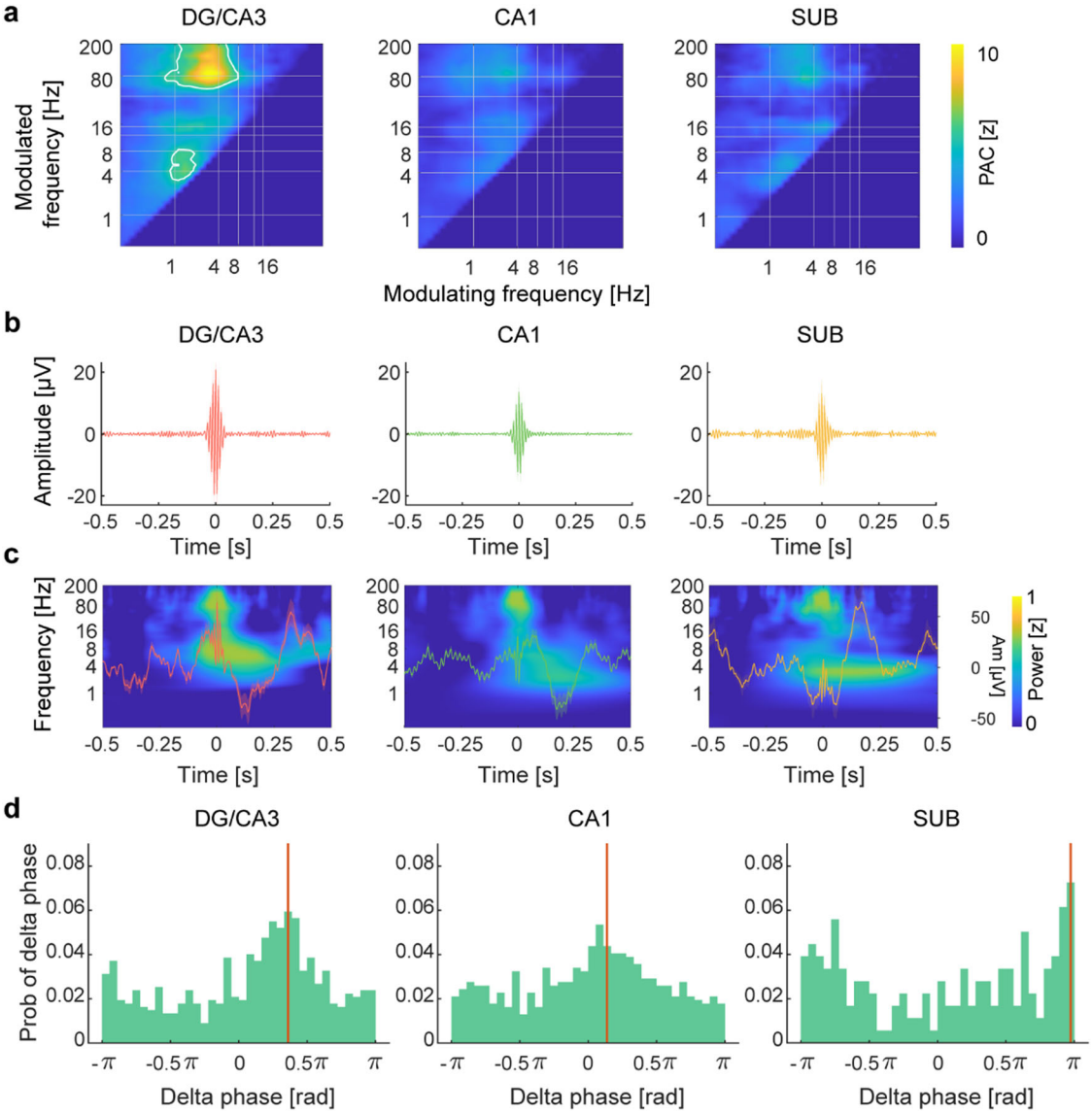

Fig. 2 | Cross-frequency coupling within each hippocampal subfield. a Phase-amplitude coupling (PAC) for DG/CA3, CA1, and SUB (white solid line circled areas indicate significant clusters: $p < 0.05$, corrected). **b** Ripple-locked grand average band-bass filtered signal in DG/CA3, CA1, and SUB (±0.5 s; mean ± SEM). **c** Ripple-locked grand average raw signal and time-frequency spectrogram in DG/CA3, CA1, and SUB (±0.5 s; mean ± SEM). **d** Probability of delta phase corresponding to the maximum ripple. The red vertical lines represent significant coupling phases (*Rayleigh*-test, Bonferroni correction, $p < 0.001$). All error bars indicate the mean ± SEM.

synaptic strength in cortical circuits could be reflected by changes in slow-wave slope[45,67–71]. We therefore measured the slope of delta oscillations in each hippocampal subfield and evaluated its changes as a function of the spindle and ripple power. The delta-wave slope was defined as the amplitude over time calculated by the straight line connecting the most negative peak of the signal with the following zero crossing (Fig. 5a). Results showed that delta slope correlated significantly with the power of spindle activity in all three hippocampal subfields (Spearman's correlation, $rs > 0.9$, $ps < 0.001$, Bonferroni corrected; Fig. 5b). In contrast, changes in ripple power only affected delta slope when ripples were at their peak amplitude (Fig. 5c). To investigate this further, we measured delta slope within ±1.5 s of ripple events and found that the delta slope was significantly higher at the peak of ripple events compared to pre-event baseline (cluster-based permutation test, $p < 0.05$; Fig. 5d).

Discussion

Our results demonstrated that during the NREM sleep, delta and spindle activities are the dominant spectral signatures in the hippocampus subfields. These two cardinal rhythms regulate high-frequency oscillations such as the ripple events in different hippocampal subfields, either individually or in conjunction. Specially, the DG/CA3 showed prominent delta-ripple coupling with all hippocampal subfields including itself, while the CA1 and SUB exhibited event-level triple coordination between the delta, spindle and ripple rhythms. Furthermore, we found that in all three hippocampal subfields, the synaptic plasticity appeared to be modulated by spindle and ripple events in a distinct fashion. Overall, our results suggest that via different layers of synchronized sleep oscillations, hippocampal subfields may play specialized roles in information communication and synaptic plasticity during NREM sleep.

NREM sleep is characterized by high slow-wave activity, consisting of the slow oscillations and delta waves. Previous studies have reported the existence of SOs in the hippocampus[21,72], but with lower amplitude and lagging peak activity compared to cortical regions[72]. In support of these earlier observations, we did not find high power in the SO frequency band in any subfield of the hippocampus, which indicates that the SOs may not be the dominating slow-wave activity in the hippocampus. Instead, we found that the hippocampus exhibited a prominent high power of delta band

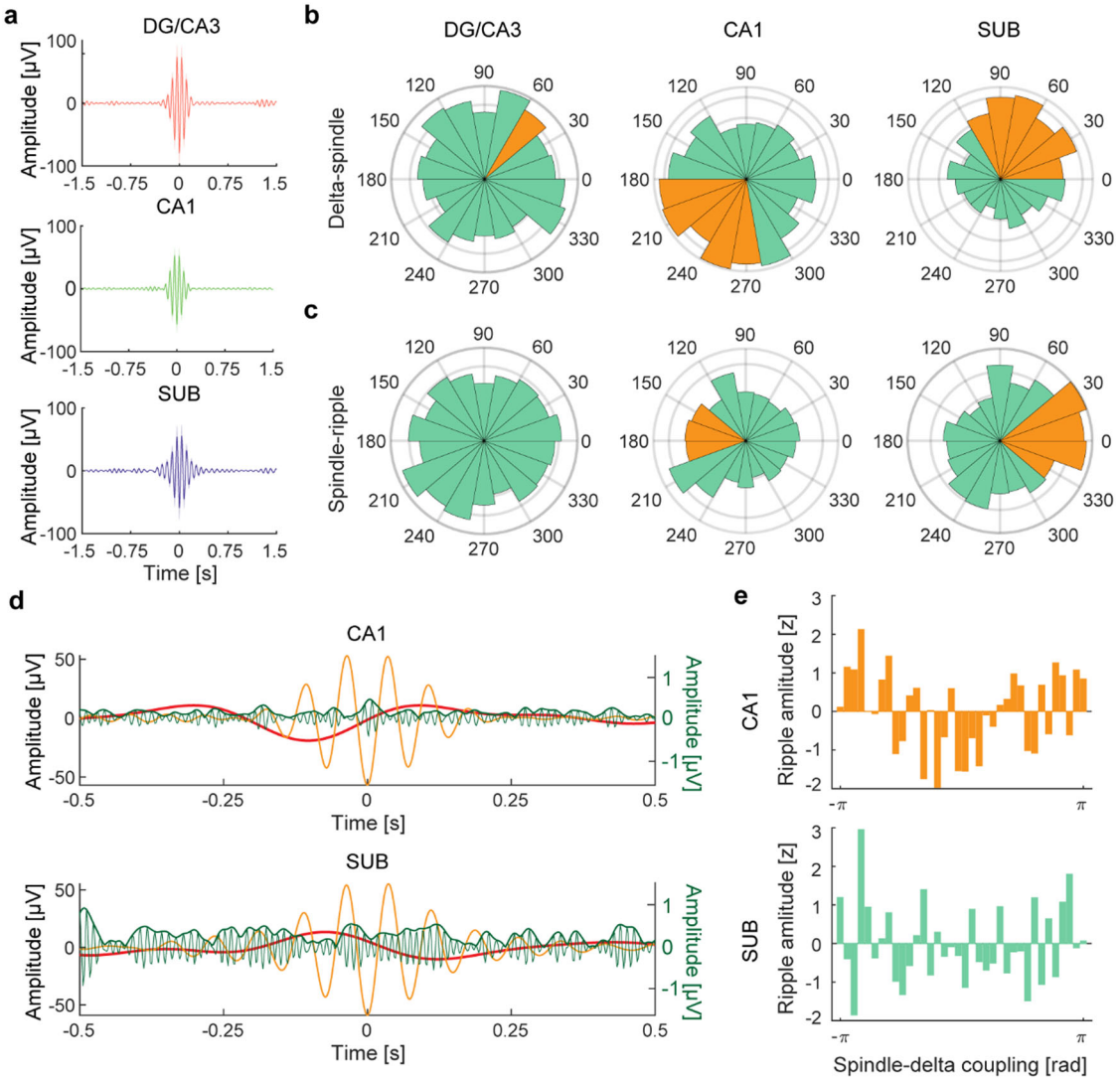

Fig. 3 | Delta-spindle-ripple coupling in hippocampal subfields. a Spindle-locked grand average band-bass filtered signal in DG/CA3, CA1, and SUB (±1.5 s; mean ± SEM). **b** Normalized histogram (18 bins, 20° each) of preferred delta-spindle modulation phases across all detected spindle events (yellow bars represent significant coupling phase ranges; *V*-test, Bonferroni correction, $p < 0.05$). **c** Normalized histogram (18 bins, 20° each) of preferred spindle-ripple modulation phases across all detected spindle events (yellow bars represent significant coupling phase ranges; *V*-test, Bonferroni correction, $p < 0.05$). **d** Average delta, spindle, ripple (and ripple's analytical amplitude), zoomed in from −0.5 s to +0.5 s to illustrate the nesting of delta-spindle-ripple in CA1 and SUB. The ripple and its analytical amplitude were scaled up by a factor of 30 for better visualization. **e** Ripple activity in CA1 and SUB as a function of the delta-spindle coupling phase. CA1 showed a significant correlation (correlation between one circular and one linear random variable; $r = 0.56$, $p = 0.0037$).

activity. Moreover, our results indicated that regardless of whether it was band-based or event-based coupling analysis, the coupling between SO and spindles/ripples in different subfields of the hippocampus during NREM sleep was comparatively weaker than the coupling between delta waves and spindles/ripples. Although both SOs and delta waves have been found to be important in modulating higher frequency rhythms (e.g., spindles and ripples)[73–75], recent studies have reported that compared to SO-ripple coupling within the cortex, hippocampal ripples appear to prefer to couple with delta activity[21,60]. This robust delta band activity may reflect the occurrence of sharp waves (even extending up to 10 Hz), which are large-amplitude synchronized-onset waves that constitute as hallmark LFP signature in the hippocampus during NREM sleep. Animal neurophysiology studies have suggested that spontaneous synchronous bursts of CA3 pyramidal neurons trigger a massive activation of CA1 and subicular pyramidal cells, as well as dentate granular cells, creating the sharp waves in these regions, which, in turn, give rise to the ripple event[76,77]. Although our ripple event-locked analysis aligns with the sharp-wave ripple complex pattern, displaying ripples atop sharp waves in all three hippocampal subfields, additional research is necessary to verify whether high delta activity in the hippocampus indeed corresponds to sharp waves or reflect other physiological phenomena.

Our study revealed distinct rhythmic synchronization profiles within the hippocampus, particularly in the DG/CA3 and CA1 subfields during NREM sleep. These different coupling patterns in the hippocampal subfields indicate their dissociable roles in information routing and processing. Specially, the DG/CA3 appears to process information in a more global manner, while the CA1 may handle more precise information processing that relies on intricate modulations to integrate current input with previously stored representations.

Several lines of our observations suggest that the DG/CA3 subfield may play a more global coordination role. Firstly, we showed that the DG/CA3 subfield exhibited robust delta-ripple coupling, while in the CA1 and SUB fields, significant delta-ripple PAC was only noticeable in event-locked analysis. Secondly, the DG/CA3 appeared to show strong delta-ripple coupling with extensive hippocampal subfields. Thirdly, although earlier research on the hippocampus as a whole identified prominent delta-spindle-

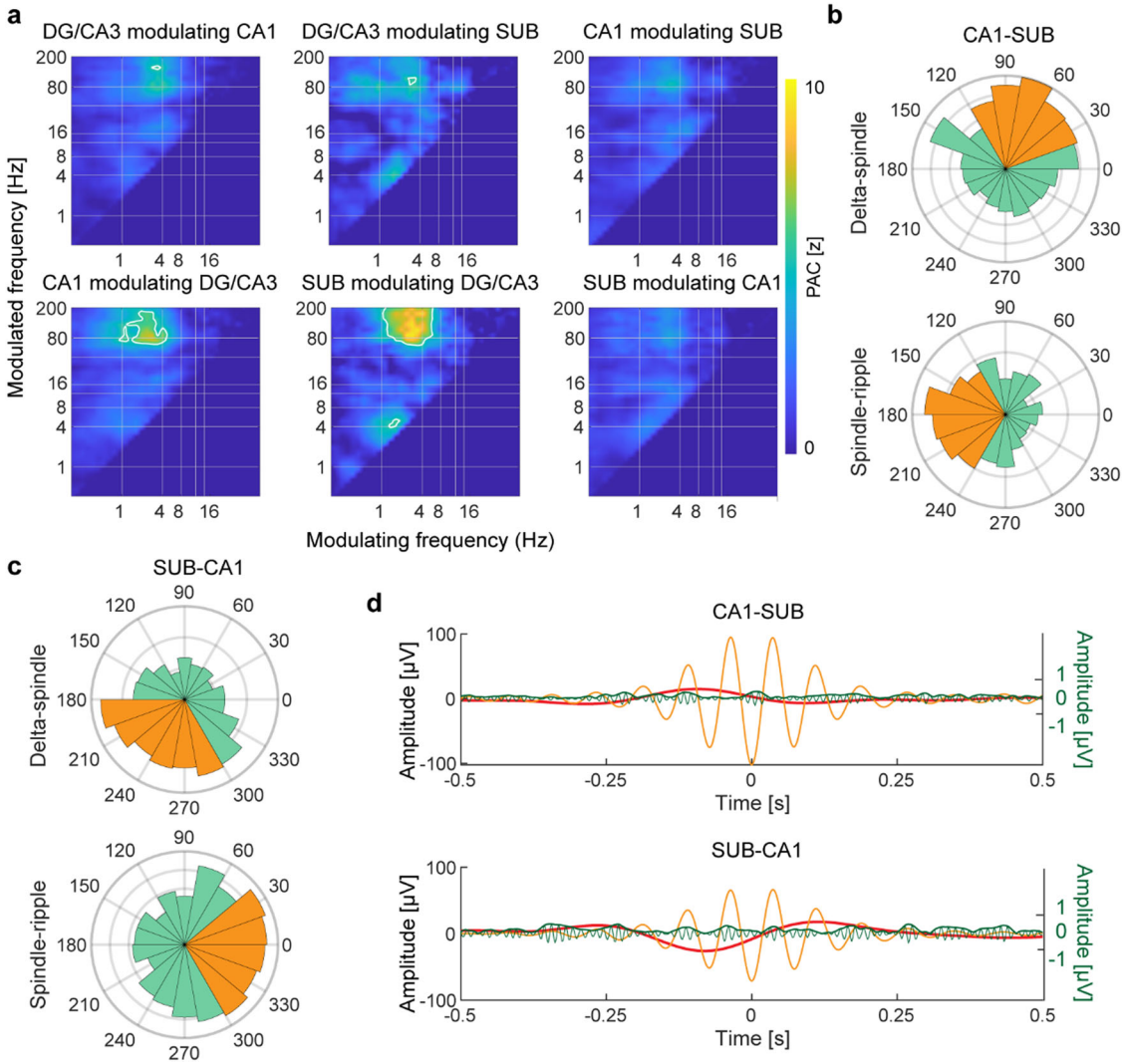

Fig. 4 | Cross-frequency coupling between hippocampal subfields. a Phase-amplitude coupling (PAC) between various hippocampal subfields. DG/CA3 exhibited significant coupling with CA1 and SUB, with the frequency range primarily concentrated in the delta-ripple, ($p < 0.05$, corrected). **b** and **c** are spindle-based event couplings. **b** Normalized histogram (18 bins, 20° each) of preferred delta-spindle (top) and spindle-ripple (bottom) modulation phases between CA1 and SUB based on CA1 spindles (yellow bars represent significant coupling phase ranges; *V*-test, Bonferroni correction, $p < 0.05$). **c** Normalized histogram of preferred phases between CA1 and SUB based on SUB spindles (yellow bars represent significant coupling phase ranges; *V*-test, Bonferroni correction, $p < 0.05$). **d** Average delta, spindle, ripple (and ripple's analytical amplitude), zoomed in from −0.5 s to +0.5 s to illustrate the nesting of delta-spindle-ripple between CA1 and SUB. The ripple and its analytical amplitude were scaled up by a factor of 30 for better visualization.

ripple trifecta coordination during NREM sleep[21,60,78], our current data suggested that this classic spindle-mediated coupling pattern was only evident in the CA1 and SUB regions but not in the DG/CA3 subfield. Collectively, these findings collectively indicate that the DG/CA3 employs a delta-ripple coupling mechanism to facilitate communication with the CA1 and SUB on a more global scale. In support of our findings, a recent study that recorded local field potentials along the dorsal CA-DG axis from sleeping mice found that the DG subfield displayed delta-band centered sharp waves strongly correlated with CA1 ripples[77]. When paired with DG sharp waves, the ripples exhibited higher amplitude and frequency compared to unpaired ripples, indicating synchronized occurrence over larger distances along the hippocampus[79]. Building on these findings, our results provide evidence in humans for the regulatory role played by the DG/CA3 subfield in modulating information flow within the hippocampal circuits during NREM sleep.

In contrast to the global delta-ripple coupling in the DG/CA3 subfield, CA1 and SUB exhibited prominent event-locked synchronization patterns involving the delta, spindle and ripple events. Although delta-spindle and spindle-ripple couplings are frequently observed in the hippocampus during NREM sleep, a closer examination reveals that they mostly occur in an event-based manner[21,60], which is in line with our data. The key difference between event-based coupling and band-based PAC lies in the time scale: event-based coupling reflects coupling strength within a short time window associated with specific events, while band-based PAC represents an average over a longer time scale (>4 s epoch in our analysis). Hence, our findings indicate that the coordination of delta, spindle and ripple rhythms in the CA1 subfield may be intermittently rather than continuous during NREM sleep, with spindle events occur sporadically during delta waves and ripples fire sporadically during spindles.

Consistent with the complementary roles of the DG/CA3 and CA1 subfields in modulating information processing observed in our study, previous research has shown that while the occurrence of DG sharp waves increased significantly following memory tasks that rely on the hippocampus, the generation of CA1 SWRs was only partially modulated[77]. Based on these observations, it has been postulated that during NREM sleep, CA1 may be involved in local information processing, while DG could serve as an indicator of coordinated information transfer between different hippocampal subfields[27,80]. The reasons why such complementary relationships

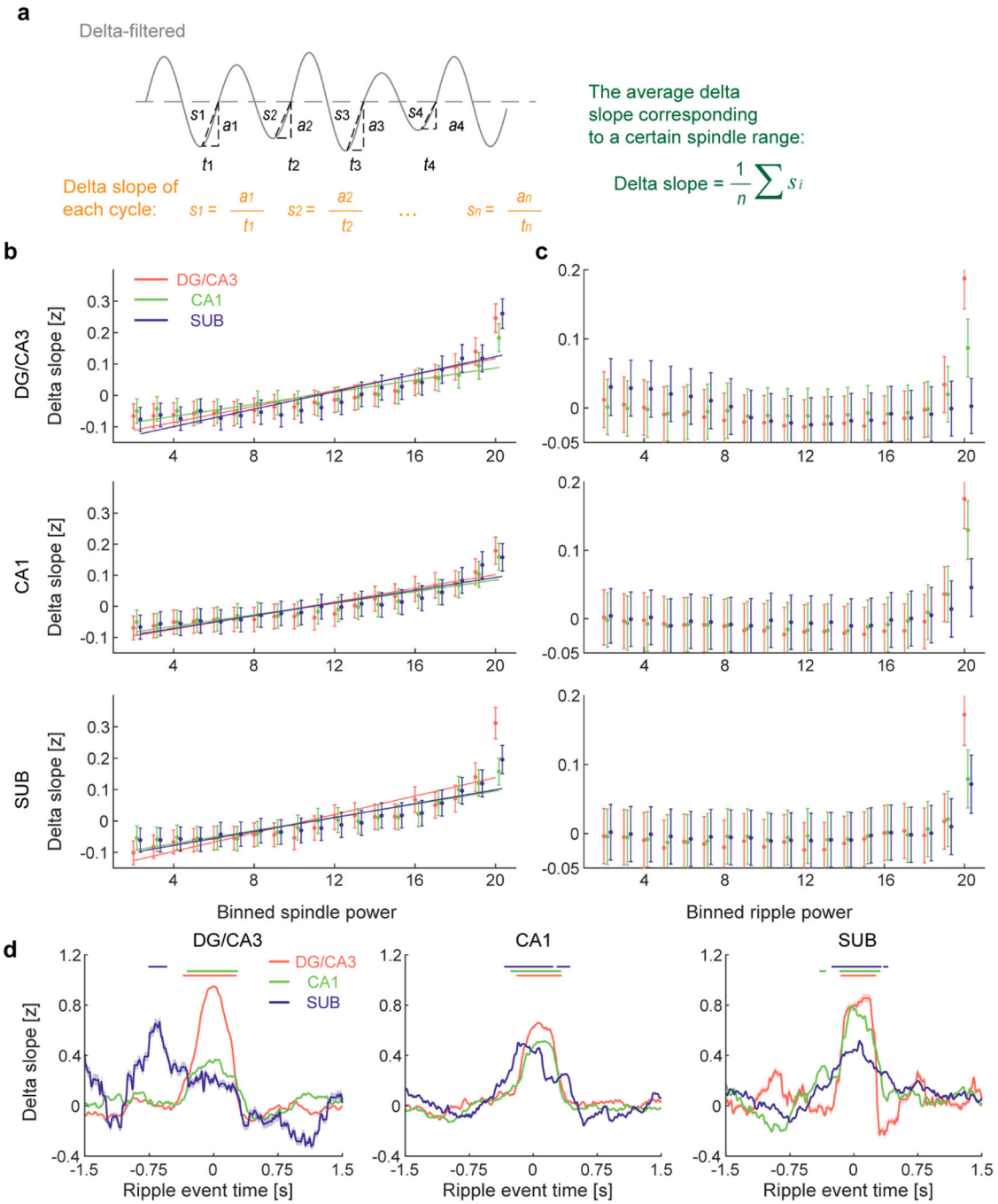

Fig. 5 | Delta slope in the hippocampus in relation to spindle and ripple. **a** Calculation method for the delta slope. Within each cycle, delta-wave slope was defined as the amplitude over time calculated by the straight line connecting the most negative peak of the signal with the following zero crossing. Then, the mean was taken over the groups. We calculated both the ascending and descending slopes, but as they yielded similar results, we only reported the results for the ascending slope. **b** Relationships between spindle power in each hippocampal subfield and delta slope in all subfields (Spearman's correlation; all subfields showed a significant positive correlation with delta slope, $rs > 0.9$; $ps < 0.001$, Bonferroni corrected). Spindle power was divided into 20 bins based on the magnitude in ascending order, and we calculated the mean delta slope within the corresponding bins. Lines are standard least-squares regression line. **c** Relationships between ripple power in each hippocampal subfield and delta slope in all subfields (Spearman's correlation; Bonferroni correction; Only a few lines showed significant associations). Ripple modulation exhibits a "binary" pattern, exclusively affecting the delta slope when the ripple power reaches its maximum. **d** Time-resolved delta slope relative to the ripple event (±1.5 s, normalized to the baseline −1.5 s to −1 s). We detected significantly increased delta slope around ripple peaks (cluster-based permutation test, $p < 0.05$). All error bars indicate the mean ± SEM.

exist and their specific physiological significance require further investigation. However, we here provide a preliminary inference. The DG/CA3 plays a crucial role in pattern separation, which involves distinguishing similar inputs or stimuli by creating distinct representations[81,82]. This process enables the DG/CA3 to encode and store memories without interference. In contrast, the CA1 is implicated in pattern completion, the process of retrieving complete representations from partial input or cues, which may rely on intricate associations with previously stored representations. Through their complementary roles in global and local processing, the DG/CA3 and CA1, in conjunction with other hippocampal subfields, enable efficient integration of previously learned representations, which in turn supports systems consolidation[18,19].

Although the regulation of synaptic homeostasis in the brain implies synaptic pruning in general, it is also accompanied by local synaptic strengthening to consolidate important memories[18,19,44]. Current synaptic homeostasis theory suggests that delta activity, as a type of slow wave, can reflect changes in synaptic levels[67,83]. Here we used an indirect index, delta-wave slope, to investigate the synaptic changes in the three subfields of the hippocampus. Overall, our findings suggest that synaptic activity within the hippocampus is heightened during moments of high spindle and ripple power in NREM sleep. This is consistent with current theories that propose spindle and ripple rhythms may directly participate in the regulation of memory at the synaptic level[4,61].

More importantly, we found that unlike the gradual modulation seen with spindle activity, ripple events exhibit a more "binary" mode of modulation, with synaptic enhancement occurring only when hippocampal ripple amplitudes are at their maximum. This may be related to the regulation scale of the spindle and ripple. According to the current neural oscillation regulation theory, different frequency bands represent different regulation scales[33,84,85]. Spindles, as relatively slow oscillations, have a wide range of regulatory effects. In contrast, ripple regulation is more precise and direct, allowing for direct interaction with neuronal replay[86] and synaptic remodeling[7]. This is consistent with the existing electrophysiological literature, which has shown direct effects triggered by the occurrence of ripples. This includes, for instance, the relationship between ripple density and memory[6,87,88] and the neural replay during ripple events[86]. In contrast, the effect of spindles on synapses is reflected in both band-based[53,72,89,90] and event-based[91,92] dynamics, indicating a more relaxed modulation effect comparing with ripples. Taking together, the spindles may provide a time window as a prerequisite for synaptic upscaling, while ripples play a more precise regulatory role in initiating synaptic upscaling.

While hippocampal oscillations are thought to play a key role in memory consolidation, there have limited knowledge regarding the coordinated rhythmic activity among different human hippocampal subfields. Through investigating the coupling relationships between oscillations in DG/CA3, CA1, and SUB of the hippocampus, we discovered that these subfields of the hippocampus complement and regulate each other, effectively promoting information processing. These findings provide valuable insights into the circuitry of the human hippocampus during NREM sleep and enhance our understanding of its role in facilitating memory consolidation.

Materials and methods

Participants

We analyzed iEEG recordings from 25 subjects with medication-resistant epilepsy (23.47 ± 8.22; Mean ± SD; 10 females) who underwent presurgical monitoring with implanted depth electrodes (Sinovation (Beijing) Medical Technology Co., length = 2 mm, diameter = 0.8 mm, center-to-center inter-contact distance = 3.5 mm, contact number 8 to16) from Sanbo Brain Hospital of Capital Medical University. Depth electrodes were implanted to localize the seizure onset zone, and the electrode targets and implantation durations were chosen entirely on clinical grounds. iEEG recording from patients who had minimal pathology and electrodes implanted in the hippocampus were used for analyses. All the patients provided written informed consent for data usage, and the study was approved by the Institutional Review Board at Sanbo Brain Hospital of Capital Medical University.

Electrode localization

To localize the electrodes[57], we first aligned the preoperative structural MRI to the ACPC coordinate system, and segmented hippocampal subfields with FreeSurfer 7.1.1 using a probabilistic atlas built with ultra-high resolution ex vivo MRI data[93–95]. After aligning the postoperative CT to the CTF head surface coordinate system, we fused the CT with the processed MRI using a rigid-body transformation in SPM. The successful fusion would show tight interlocking of CT-positive skull and MRI-positive brain and skin tissue. After importing the header information including the list of electrode labels from iEEG data, we obtained the electrode coordinates and were able to determine whether electrodes were located in DG/CA3, CA1, and SUB based on the probabilistic hippocampal atlas from the FreeSurfer segmentation. As DG, CA3, and CA4 are anatomically close, electrodes categorized as DG/CA3 in this study also encompassed CA4. The above operations are all based on the Fieldtrip toolbox[96] in MatLab 2020a (MathWorks Inc.). Two independent neurologists also visually determined electrode positions based on individual scans in native space. After excluding noisy channels, we obtained a total of 71 electrode contacts in DG/CA3, CA1, and SUB. Please refer to Supplementary Table 2 for details.

Data preprocessing and NREM sleep selection

Data analysis was performed using MatLab 2020a (MathWorks Inc.) with custom-written code, supplemented by relevant functions from the FieldTrip toolbox[96], the EEGLAB toolbox[97], and the CircStat toolbox[98]. In every subject ($N = 25$), the selected electrodes were notch-filtered at 50 Hz and its harmonics, bipolar referenced to its immediate lateral neighboring electrode, and down-sampled to 512 Hz. All resulting traces were manually inspected to exclude noisy, epileptic and artifact-contaminated hippocampus channels. A detailed description of the confirmation of interictal epileptic discharges is provided below.

Due to the unavailability of clinical hypnograms, patient monitoring videos, scalp EEG, and electrooculogram, we were unable to classify sleep stages according to the criteria by the American Academy of Sleep Medicine (AASM). Instead, we identified NREM sleep (including N2 and N3, but excluding N1) by adopting methods from a previous iEEG study[58,59]. Specifically, we extracted the iEEG recordings from nights that were confirmed by a neurologist to be seizure-free. NREM sleep was identified as a prolonged time period that are characterized by increased activity amplitude in the low delta frequency band (<2 Hz), and decreased amplitude in the high gamma frequency band (70–190 Hz) and an initially high but gradually decreasing amplitude in the spindle frequency band (9–17 Hz). When selecting NREM epochs for sleep staging, we focused solely on the electrodes located in the neocortex. NREM sleep was identified only if the majority of these neocortical electrodes met the aforementioned criteria. Each NREM period was then visually inspected to confirm the presence of NREM sleep graphoelements. We retained time periods for which we had sufficient confidence in ensuring the accuracy of NREM sleep determination.

Interictal epileptic discharge (IED) detection

Prior to all analyses, we first detected IEDs using an automated algorithm[99,100] on all contacts located in the hippocampus. The iEEG signal was bandpass filtered between 25 and 80 Hz. Hilbert transform was applied to obtain the envelope amplitude, which was subsequently z-scored. Events were recognized when this signal was 3 SD above the mean for >20 ms and <100 ms. The IED events were then time-locked to the peak and the ±2.5 s before and after the peak was considered as an artifact (Supplementary Fig. 1). A subset of events was sampled and verified through visual examination by two neurologists. If a single channel displayed an artifact, that data segment would not be included for any of the channels, further reducing the likelihood of pathological activity. The removed time range was ±5 s of the IED peaks.

Spectral analysis

To obtain the spectra of the three hippocampal subfields, we utilized the Welch's method, applying a Hamming window of 4 s with an 80% overlap[60]. We also normalized the spectra by computing z-scores along the frequency domain.

Time-frequency analysis

To obtain continuous time-frequency representations for all artifact-free epochs, the initial signals underwent wavelet analysis[60] within the frequency range of 0.2 to 200 Hz, encompassing 50 logarithmically spaced frequencies. Each epoch was extended with 5 s on either side to minimize edge artifacts.

Wavelets were defined in terms of desired temporal resolution according to Eq. (1):

$$wavelet = e^{i2\pi tf} * e^{-4\ln(2)t^2/h^2} \quad (1)$$

where i is the imaginary operator, t is time in seconds, f is frequency (50 logarithmically spaced frequencies between 0.5 and 200 Hz), ln is the natural logarithm, and h is temporal resolution (logarithmically spaced between 3 s and 0.025 s). Spectrograms showed the z-scored power across times in each frequency point.

Band-based cross-frequency coupling

Phase-amplitude coupling (PAC) analysis was conducted using the Mean Vector Length (MLV) method[60,62]. For every epoch, all pairs of modulating frequency $f1$ and modulated frequency $f2$ came from the wavelet analysis (Eq. (1)), and $f2 > 2*f1$. To adjust the possible bias stemming from non-sinusoidal shapes, we calculated complex-valued debiased phase-amplitude coupling (dPAC) according to Eqs. (2, 3)[101]:

$$dPAC = \frac{1}{n}\sum_{t=1}^{n}\left(ampf2(t)*(e^{i\phi f1(t)} - B)\right) \quad (2)$$

$$B = \frac{1}{n}\sum_{t=1}^{n} e^{i\phi f1(t)} \quad (3)$$

where i is the imaginary operator, t is time in seconds, $amp_{f2}(t)$ is the amplitude of $f2$, $\phi_{f1}(t)$ is the phase of $f1$ ($f1, f2$ from 0.2 to 200 Hz, $f2 > 2*f1$).

Subsequently, we generated a surrogate distribution of coupling strengths by iteratively shifting the $f1$ phase time series with respect to the $f2$ amplitude time series by a random amount (repeated 500 times) and recalculated the Mean Vector Length for each iteration. The observed coupling strength was then normalized by calculating a z-score in comparison to this null distribution of coupling strength values. All the reported analyses pertaining to coupling strength are based on this z-scored dPAC. The z-values were than transformed into p-values and significant clusters were identified when z-value > 3 × 1.64 (one-tail, $p < 0.05$, Bonferroni corrected for three subfields).

Event detection

We utilized previously established detection algorithms[21,102] to identify spindle and ripple events from hippocampal electrodes. We randomly sampled a subset of the detected events and subjected them to visual examination by a neurologist. Only artifact-free data from NREM sleep stages were employed for event detection.

To detect spindles, for each electrode, we filtered the raw signal between 12–16 Hz and calculated the filtered signal's root mean square (RMS) utilizing a moving average of 200 ms. We defined the spindle amplitude criterion as the 75th percentile of RMS values. A spindle event was detected whenever the signal exceeded this threshold for more than 0.5 s but less than 3 s. Artifact-free epochs (−2.5 s to +2.5 s) time-locked to the maximum spindle trough in the filtered signal were extracted from the unfiltered raw signal for all events.

To detect ripples, we filtered the raw signal from each electrode within the 80–100 Hz and calculated the filtered signal's RMS utilizing a moving average of 20 ms. We defined the ripple amplitude criterion as the 99th percentile of RMS values. A ripple event was detected whenever the signal exceeded this threshold for a minimum of 38 ms. Additionally, we required at least 3 discrete peaks or 3 discrete troughs to occur in the raw signal segment corresponding to the above-threshold RMS segment. Artifact-free epochs (−1.5 s to +1.5 s) time-locked to the maximum ripple peak in the filtered signal were extracted from the unfiltered raw signal for all events.

Event-based cross-frequency coupling

For each detected spindle event epoch, we used preferred PAC phases method to measure the event-based coupling[21]. We first filtered the raw signals for frequencies of interest (SO: 0.2–1 Hz; delta: 1–4 Hz; spindle: 12–16 Hz; ripple: 80–100 Hz) within the spindle event epoch. Then, we utilized the Hilbert transform to extract the phase values of the lower-frequency oscillation (modulating) and the phase values of the power fluctuation of the higher-frequency oscillation (modulated). Finally, we calculated the coupling phase by evaluating the angle of the synchronization index (SI) between the two phase value time series (modulating and modulated) for each event epoch. SI is a complex number of which the angle represents the 'preferred phase' of the synchronization (SIp), that is, the phase of the lower frequency at which the power of the higher frequency is maximal across time:

$$SI = \frac{1}{n}\sum_{t=1}^{n} e^{i^*\left(\phi_l(t) - \phi_u(t)\right)} \quad (4)$$

where n is the number of time points, i is the imaginary operator, $\phi_u(t)$ is the phase value of the higher frequency power fluctuation at time point t, and $\phi_l(t)$ is the phase value of the lower frequency signal at time point t. The time intervals for estimating the preferred phase were −1 s to +1 s around the spindle center for delta-spindle coupling and −0.25 s to +0.25 s around the spindle center for spindle-ripple coupling.

Ripple activity as a function of delta-spindle coupling phase

To further analyze the delta-spindle-ripple triple coupling, we expressed the normalized ripple amplitude as a function of the precise delta-spindle coupling phase[100]. First, we determined the delta coupling phase for every spindle event and binned coupling phase into 36 nonoverlapping, 10° wide bins. Then, we time-locked the ripple activity relative to the detected spindle events and extracted the average power per bin during the spindle peak. To further quantify this relationship, we calculated a circular-linear correlation between the phase vector (36 bins) and the ripple power.

Correlation between spindle power, ripple power and delta slope

The delta-wave slope was defined as the amplitude over time calculated by the straight line connecting the most negative peak of the signal with the following zero crossing (Fig. 5a)[83]. While both the ascending and descending slopes were computed, only the results for the ascending slope are reported in this manuscript, as they yielded similar outcomes.

For every epoch, we first performed delta band filtering, and calculated the delta slope for each cycle, and assigned the delta slope value to all time points in that cycle. Then, we filtered the spindle band, and extracted the spindle power. This resulted in a delta slope sequence and a spindle power sequence that were consistent with the epoch time length. Delta slope was z-scored. We then divided the spindle sequence into 20 bins based on the magnitude of their power values, and calculated the mean delta slope within the corresponding bins. To quantitatively characterize the relationship, we calculated the Spearman correlation between spindle powers and delta slopes (20 pairs from 20 bins).

We also measured the relationship between ripple power and delta slope using the above method. Furthermore, to further assess the delta slope changes induced by the ripple event, we extracted the delta slopes within the range of the ripple event (−1.5 s to +1.5 s).

Statistics and reproducibility

Statistical analysis was performed using MatLab 2020a (MathWorks Inc.) with custom-written code and the CircStat toolbox[98]. P-values < 0.05 were considered significant unless stated otherwise. For spectral statistics, we used cluster-based permutation tests to correct for multiple comparisons (Monte Carlo method; 1000 iterations; maxsum criterion). Clusters were formed via two-tailed independent samples t-tests thresholded at $p < 0.05$ ($n = 15$ for DG/CA3, $n = 19$ for CA1, $n = 10$ for SUB). The significance of

phases of delta histogram for ripple was tested by *Rayleigh*-test[98] ($n = 673$ for DG/CA3, $n = 617$ for CA1, $n = 179$ for SUB) and phases of event-based coupling was tested by *V*-test[98] (Within hippocampal subfields: $n = 1346$ for DG/CA3, $n = 1244$ for CA1, $n = 972$ for SUB; between hippocampal subfields: $n = 556$ for SUB-CA1, $n = 622$ for CA1-SUB), and all followed by Bonferroni correction. The correlation between delta-spindle coupling phases and ripple power was calculated by a circular-linear correlation function of CircStat toolbox[98] ($n = 1244$ for CA1, $n = 972$ for SUB), and the correlation between spindle/ripple power and delta slope was calculated by Spearman's correlation ($n = 20$ bins). The delta slope within ripple event was tested against the baseline (-1.5 s to -1 s) by cluster-based permutation tests (Monte Carlo method; 1000 iterations; maxsum criterion). Clusters were formed via two-tailed one-sample *t*-tests thresholded at $p < 0.05$.

Reporting summary

Further information on research design is available in the Nature Portfolio Reporting Summary linked to this article.

Data availability

The data sets generated and analyzed here are available from the corresponding author on reasonable request. Data for all figures is available in Supplementary Data 1–5 files.

Code availability

EEG data analyses were performed in the freely available toolbox EEGLAB (2022.1, https://sccn.ucsd.edu/eeglab), FieldTrip (20211209, https://www.fieldtriptoolbox.org/) and CircStat (1.21.0.0, https://ww2.mathworks.cn/matlabcentral/fileexchange/10676-circular-statistics-toolbox-directional-statistics) in combination with custom MATLAB (R2020a, https://ww2.mathworks.cn/en/products/matlab.html) scripts. sMRI data analyses were performed in FreeSurfer (7.1.1, https://surfer.nmr.mgh.harvard.edu/) in combination with custom MATLAB script. All the computer code used to implement the experiments and to collect and analyze data is available from the corresponding author on reasonable request.

Received: 25 January 2024; Accepted: 23 September 2024;
Published online: 01 October 2024

References

1. Aeschbach, D., Cutler, A. & Ronda, J. A Role for Non-Rapid-Eye-Movement Sleep Homeostasis in Perceptual Learning. *J. Neurosci. : Off. J. Soc. Neurosci.* **28**, 2766–2772 (2008).
2. Huber, R., Felice Ghilardi, M., Massimini, M. & Tononi, G. Local sleep and learning. *Nature* **430**, 78–81 (2004).
3. Gais, S., Plihal, W., Wagner, U. & Born, J. Early sleep triggers memory for early visual discrimination skills. *Nat. Neurosci.* **3**, 1335–1339 (2000).
4. Dickey, C. W. et al. Cortical Ripples during NREM Sleep and Waking in Humans. *J. Neurosci.* **42**, 7931–7946 (2022).
5. Plihal, W. & Born, J. Effects of early and late nocturnal sleep on declarative and procedural memory. *J. Cogn. Neurosci.* **9**, 534–547 (1997).
6. Norman, Y. et al. Hippocampal sharp-wave ripples linked to visual episodic recollection in humans. *Science* **365**, eaax 1030 (2019).
7. Hall, A. F. & Wang, D. V. The two tales of hippocampal sharp-wave ripple content: The rigid and the plastic. *Prog. Neurobiol.* **221**, 102396 (2023).
8. van Schalkwijk, F. J. et al. An evolutionary conserved division-of-labor between archicortical and neocortical ripples organizes information transfer during sleep. *Prog. Neurobiol.* **227**, 102485 (2023).
9. Niethard, N., Ngo, H.-V. V., Ehrlich, I. & Born, J. Cortical circuit activity underlying sleep slow oscillations and spindles. *PNAS* **115**, E9220–E9229 (2018).
10. Latchoumane, C.-F. V., Ngo, H.-V. V., Born, J. & Shin, H.-S. Thalamic Spindles Promote Memory Formation during Sleep through Triple Phase-Locking of Cortical, Thalamic, and Hippocampal Rhythms. *Neuron* **95**, 424–435.e426 (2017).
11. Mölle, M., Bergmann, T., Marshall, L. & Born, J. Fast and Slow Spindles during the Sleep Slow Oscillation: Disparate Coalescence and Engagement in Memory Processing. *Sleep* **34**, 1411–1421 (2011).
12. Maingret, N., Girardeau, G., Todorova, R., Goutierre, M. & Zugaro, M. Hippocampo-cortical coupling mediates memory consolidation during sleep. *Nat. Neurosci.* **19**, 959–964 (2016).
13. Sirota, A., Csicsvari, J., Buhl, D. & Buzsáki, G. Communication between neocortex and hippocampus during sleep in rodents. *PNAS* **100**, 2065–2069 (2003).
14. Diekmann, N. & Cheng, S. A model of hippocampal replay driven by experience and environmental structure facilitates spatial learning. *eLife* **12**, e82301 (2023).
15. Liu, J. et al. Transformative neural representations support long-term episodic memory. *Sci. Adv.* **7**, eabg9715 (2021).
16. Liu, Y., Dolan, R. J., Kurth-Nelson, Z. & Behrens, T. E. J. Human Replay Spontaneously Reorganizes Experience. *Cell* **178**, 640–652.e614 (2019).
17. Sun, W., Advani, M., Spruston, N., Saxe, A. & Fitzgerald, J. E. Organizing memories for generalization in complementary learning systems. *Nat. Neurosci.* **26**, 1438–1448 (2023).
18. Klinzing, J. G., Niethard, N. & Born, J. Mechanisms of systems memory consolidation during sleep. *Nat. Neurosci.* **22**, 1598–1610 (2019).
19. Diekelmann, S. & Born, J. The memory function of sleep. *Nat. Rev. Neurosci.* **11**, 114–126 (2010).
20. Buzsáki, G. Hippocampal sharp wave-ripple: A cognitive biomarker for episodic memory and planning. *Hippocampus* **25**, 1073–1188 (2015).
21. Staresina, B. P. et al. Hierarchical nesting of slow oscillations, spindles and ripples in the human hippocampus during sleep. *Nat. Neurosci.* **18**, 1679–1686 (2015).
22. Moroni, F. et al. Procedural learning and sleep hippocampal low frequencies in humans. *Neuroimage* **42**, 911–918 (2008).
23. Moroni, F. et al. Slow EEG rhythms and inter-hemispheric synchronization across sleep and wakefulness in the human hippocampus. *Neuroimage* **60**, 497–504 (2012).
24. Moroni, F. et al. Hippocampal slow EEG frequencies during NREM sleep are involved in spatial memory consolidation in humans. *Hippocampus* **24**, 1157–1168 (2014).
25. Lin, X. et al. Noncanonical projections to the hippocampal CA3 regulate spatial learning and memory by modulating the feedforward hippocampal trisynaptic pathway. *PLoS Biol.* **19**, e3001127 (2021).
26. Li, S. et al. Predictable navigation through spontaneous brain states with cognitive-map-like representations. *Prog. Neurobiol.* **233**, 102570 (2024).
27. Mizuseki, K. & Kitanishi, T. Oscillation-coordinated, noise-resistant information distribution via the subiculum. *Curr. Opin. Neurobiol.* **75**, 102556 (2022).
28. Leal, S. L. & Yassa, M. A. Integrating new findings and examining clinical applications of pattern separation. *Nat. Neurosci.* **21**, 163–173 (2018).
29. Schlichting, M. L., Gumus, M., Zhu, T. & Mack, M. L. The structure of hippocampal circuitry relates to rapid category learning in humans. *Hippocampus* **31**, 1179–1190 (2021).
30. Ketz, N., Morkonda, S. G. & O'Reilly, R. C. Theta coordinated error-driven learning in the hippocampus. *PLoS Comput. Biol.* **9**, e1003067 (2013).
31. O'Mara, S. Controlling hippocampal output: The central role of subiculum in hippocampal information processing. *Behav. Brain Res.* **174**, 304–312 (2006).
32. Matsumoto, N., Kitanishi, T. & Mizuseki, K. The subiculum: Unique hippocampal hub and more. *Neurosci. Res.* **143**, 1–12 (2019).
33. Fries, P. Rhythms for Cognition: Communication through Coherence. *Neuron* **88**, 220–235 (2015).

34. Puentes-Mestril, C., Roach, J., Niethard, N., Zochowski, M. & Aton, S. J. How rhythms of the sleeping brain tune memory and synaptic plasticity. *Sleep* **42**, zsz095 (2019).
35. Zeidman, P., Lutti, A. & Maguire, E. A. Investigating the functions of subregions within anterior hippocampus. *Cortex* **73**, 240–256 (2015).
36. Zeidman, P. & Maguire, E. A. Anterior hippocampus: the anatomy of perception, imagination and episodic memory. *Nat. Rev. Neurosci.* **17**, 173–182 (2016).
37. Dimsdale-Zucker, H. R., Ritchey, M., Ekstrom, A. D., Yonelinas, A. P. & Ranganath, C. CA1 and CA3 differentially support spontaneous retrieval of episodic contexts within human hippocampal subfields. *Nat. Commun.* **9**, 294 (2018).
38. Bellesi, M. & de Vivo, L. Structural synaptic plasticity across sleep and wake. *Curr. Opin. Physiol.* **15**, 74–81 (2020).
39. Tononi, G. & Cirelli, C. Sleep and the Price of Plasticity: From Synaptic and Cellular Homeostasis to Memory Consolidation and Integration. *Neuron* **81**, 12–34 (2014).
40. de Vivo, L. et al. Ultrastructural evidence for synaptic scaling across the wake/sleep cycle. *Science* **355**, 507–510 (2017).
41. Vyazovskiy, V. V., Cirelli, C., Pfister-Genskow, M., Faraguna, U. & Tononi, G. Molecular and electrophysiological evidence for net synaptic potentiation in wake and depression in sleep. *Nat. Neurosci.* **11**, 200–208 (2008).
42. Diering, G. H. et al. Homer1a drives homeostatic scaling-down of excitatory synapses during sleep. *Science* **355**, 511–515 (2017).
43. Vyazovskiy, V. V. et al. Cortical Firing and Sleep Homeostasis. *Neuron* **63**, 865–878 (2009).
44. Brodt, S., Inostroza, M., Niethard, N. & Born, J. Sleep—A brain-state serving systems memory consolidation. *Neuron* **111**, 1050–1075 (2023).
45. Knyazev, G. G. EEG delta oscillations as a correlate of basic homeostatic and motivational processes. *Neurosci. Biobehav. Rev.* **36**, 677–695 (2012).
46. Assenza, G., Pellegrino, G., Tombini, M., Di Pino, G. & Di Lazzaro, V. Wakefulness delta waves increase after cortical plasticity induction. *Clin. Neurophysiol.* **126**, 1221–1227 (2015).
47. Steriade, M., Timofeev, I. & Grenier, F. Natural Waking and Sleep States: A View From Inside Neocortical Neurons. *J. Neurophysiol.* **85**, 1969–1985 (2001).
48. Massimini, M., Huber, R., Ferrarelli, F., Hill, S. L. & Tononi, G. J. T. J. O. N. The Sleep Slow Oscillation as a Traveling Wave. *J. Neurosci.* **24**, 6862–6870 (2004).
49. Marshall, L., Helgadóttir, H., Mölle, M. & Born, J. Boosting slow oscillations during sleep potentiates memory. *Nature* **444**, 610–613 (2006).
50. Esfahani, M. J. et al. Closed-loop auditory stimulation of sleep slow oscillations: Basic principles and best practices. *Neurosci. Biobehav. Rev.* **153**, 105379 (2023).
51. Riedner, B. et al. Sleep Homeostasis and Cortical Synchronization: III. A High-Density EEG Study of Sleep Slow Waves in Humans. *Sleep* **30**, 1643–1657 (2008).
52. Rosanova, M. & Ulrich, D. Pattern-specific associative long-term potentiation induced by a sleep spindle-related spike train. *J. Neurosci.* **25**, 9398–9405 (2005).
53. Seibt, J. et al. Cortical dendritic activity correlates with spindle-rich oscillations during sleep in rodents. *Nat. Commun.* **8**, 684 (2017).
54. Wierzynski, C. M., Lubenov, E. V., Gu, M. & Siapas, A. G. State-Dependent Spike-Timing Relationships between Hippocampal and Prefrontal Circuits during Sleep. *Neuron* **61**, 587–596 (2009).
55. Barnes, C. et al. LTP saturation and spatial learning disruption: effects of task variables and saturation levels. *J. Neurosci. Methods* **14**, 5793–5806 (1994).
56. Buzsáki, G. Long-term changes of hippocampal sharp-waves following high frequency afferent activation. *Brain Res* **300**, 179–182 (1984).
57. Stolk, A. et al. Integrated analysis of anatomical and electrophysiological human intracranial data. *Nat. Protoc.* **13**, 1699–1723 (2018).
58. Jiang, X. et al. Replay of large-scale spatio-temporal patterns from waking during subsequent NREM sleep in human cortex. *Sci. Rep.* **7**, 17380 (2017).
59. Jiang, X. et al. Improved identification and differentiation from epileptiform activity of human hippocampal sharp wave ripples during NREM sleep. *Hippocampus* **30**, 610–622 (2020).
60. Cox, R., Rüber, T., Staresina, B. P. & Fell, J. Heterogeneous profiles of coupled sleep oscillations in human hippocampus. *Neuroimage* **202**, 116178 (2019).
61. Gonzalez, C., Jiang, X., Gonzalez-Martinez, J. & Halgren, E. Human Spindle Variability. *J. Neurosci.* **42**, 4517–4537 (2022).
62. Canolty, R. T. et al. High gamma power is phase-locked to theta oscillations in human neocortex. *Science* **313**, 1626–1628 (2006).
63. Skelin, I. et al. Coupling between slow waves and sharp-wave ripples engages distributed neural activity during sleep in humans. *PNAS* **118**, e2012075118 (2021).
64. Jiang, X., Gonzalez-Martinez, J. & Halgren, E. Coordination of Human Hippocampal Sharpwave Ripples during NREM Sleep with Cortical Theta Bursts, Spindles, Downstates, and Upstates. *J. Neurosci.* **39**, 8744–8761 (2019).
65. Liu, A. A. et al. A consensus statement on detection of hippocampal sharp wave ripples and differentiation from other fast oscillations. *Nat. Commun.* **13**, 6000 (2022).
66. Deadwyler, S. A. & Hampson, R. E. Differential but Complementary Mnemonic Functions of the Hippocampus and Subiculum. *Neuron* **42**, 465–476 (2004).
67. Tononi, G. & Cirelli, C. Steep function and synaptic homeostasis. *Sleep. Med. Rev.* **10**, 49–62 (2006).
68. Esser, S. K., Hill, S. & Tononi, G. Sleep Homeostasis and Cortical Synchronization: I. Modeling the Effects of Synaptic Strength on Sleep Slow Waves. *Sleep* **30**, 1617–1630 (2008).
69. Borbély, A. A. A two process model of sleep regulation. *Hum. Neurobiol.* **1**, 195–204 (1982).
70. Borbely, A. A. From slow waves to sleep homeostasis: New perspectives. *Arch. italiennes de. biologie* **139**, 53–61 (2001).
71. Assenza, G. & Di Lazzaro, V. A useful electroencephalography (EEG) marker of brain plasticity: delta waves. *Neural Regen. Res* **10**, 1216–1217 (2015).
72. Nir, Y. et al. Regional slow waves and spindles in human sleep. *Neuron* **70**, 153–169 (2011).
73. Kim, J., Gulati, T. & Ganguly, K. Competing Roles of Slow Oscillations and Delta Waves in Memory Consolidation versus Forgetting. *Cell* **179**, 514–526.e513 (2019).
74. Cox, R., Rüber, T., Staresina, B. P. & Fell, J. Phase-based coordination of hippocampal and neocortical oscillations during human sleep. *Commun. Biol.* **3**, 176 (2020).
75. Sanda, P. et al. Bidirectional Interaction of Hippocampal Ripples and Cortical Slow Waves Leads to Coordinated Spiking Activity During NREM Sleep. *Cereb. Cortex* **31**, 324–340 (2021).
76. Buzsáki, G. Hippocampal sharp waves: Their origin and significance. *Brain Res* **398**, 242–252 (1986).
77. Meier, K., Merseburg, A., Isbrandt, D., Marguet, S. L. & Morellini, F. Dentate Gyrus Sharp Waves, a Local Field Potential Correlate of Learning in the Dentate Gyrus of Mice. *J. Neurosci.* **40**, 7105–7118 (2020).
78. Girardeau, G. & Lopes-Dos-Santos, V. Brain neural patterns and the memory function of sleep. *Science* **374**, 560–564 (2021).
79. Patel, J., Schomburg, E. W., Berenyi, A., Fujisawa, S. & Buzsaki, G. Local Generation and Propagation of Ripples along the Septotemporal Axis of the Hippocampus. *J. Neurosci.* **33**, 17029–17041 (2013).
80. Hainmueller, T. & Bartos, M. Dentate gyrus circuits for encoding, retrieval and discrimination of episodic memories. *Nat. Rev. Neurosci.* **21**, 153–168 (2020).

81. Treves, A. & Rolls, E. T. Computational constraints suggest the need for two distinct input systems to the hippocampal CA3 network. *Hippocampus* **2**, 189–199 (1992).
82. Bakker, A., Kirwan, C. B., Miller, M. & Stark, C. E. Pattern separation in the human hippocampal CA3 and dentate gyrus. *Science* **319**, 1640–1642 (2008).
83. Kurth, S. et al. Characteristics of sleep slow waves in children and adolescents. *Sleep* **33**, 475–480 (2010).
84. Buzsaki, G. & Voroslakos, M. Brain rhythms have come of age. *Neuron* **111**, 922–926 (2023).
85. Deng, X. et al. A Variable Clock Underlies Internally Generated Hippocampal Sequences. *J. Neurosci.* **42**, 3797–3810 (2022).
86. Diba, K. & Buzsaki, G. Forward and reverse hippocampal place-cell sequences during ripples. *Nat. Neurosci.* **10**, 1241–1242 (2007).
87. Norman, Y., Raccah, O., Liu, S., Parvizi, J. & Malach, R. Hippocampal ripples and their coordinated dialogue with the default mode network during recent and remote recollection. *Neuron* **109**, 2767–2780.e2765 (2021).
88. Duan, Q.-T. et al. Hippocampal ripples correlate with memory performance in humans. *Brain Res* **1810**, 148370 (2023).
89. Varma, S., Daselaar, S. M., Kessels, R. P. C. & Takashima, A. Promotion and suppression of autobiographical thinking differentially affect episodic memory consolidation. *PLoS One* **13**, e0201780 (2018).
90. Ribeiro, S. et al. Novel experience induces persistent sleep-dependent plasticity in the cortex but not in the hippocampus. *Front. Neurosci.* **1**, 43–55 (2007).
91. Gais, S., Mölle, M., Helms, K. & Born, J. Learning-dependent increases in sleep spindle density. *J. Neurosci.* **22**, 6830–6834 (2002).
92. Bergmann, T. O., Mölle, M., Diedrichs, J., Born, J. & Siebner, H. R. Sleep spindle-related reactivation of category-specific cortical regions after learning face-scene associations. *NeuroImage* **59**, 2733–2742 (2012).
93. Iglesias, J. E. et al. A computational atlas of the hippocampal formation using ex vivo, ultra-high resolution MRI: Application to adaptive segmentation of in vivo MRI. *NeuroImage* **115**, 117–137 (2015).
94. Saygin, Z. M. et al. High-resolution magnetic resonance imaging reveals nuclei of the human amygdala: manual segmentation to automatic atlas. *NeuroImage* **155**, 370–382 (2017).
95. Iglesias, J. E. et al. Bayesian longitudinal segmentation of hippocampal substructures in brain MRI using subject-specific atlases. *NeuroImage* **141**, 542–555 (2016).
96. Oostenveld, R., Fries, P., Maris, E. & Schoffelen, J.-M. FieldTrip: Open Source Software for Advanced Analysis of MEG, EEG, and Invasive Electrophysiological Data. *Comput. Intell. Neurosci.* **2011**, 156869 (2011).
97. Delorme, A. & Makeig, S. EEGLAB: an open source toolbox for analysis of single-trial EEG dynamics including independent component analysis. *J. Neurosci. Methods* **134**, 9–21 (2004).
98. Berens, P. CircStat: A MATLAB Toolbox for Circular Statistics. *J. Stat. Softw.* **31**, 1–21 (2009).
99. Gelinas, J. N., Khodagholy, D., Thesen, T., Devinsky, O. & Buzsáki, G. Interictal epileptiform discharges induce hippocampal–cortical coupling in temporal lobe epilepsy. *Nat. Med.* **22**, 641–648 (2016).
100. Helfrich, R. F. et al. Bidirectional prefrontal-hippocampal dynamics organize information transfer during sleep in humans. *Nat. Commun.* **10**, 3572 (2019).
101. van Driel, J., Cox, R. & Cohen, M. X. Phase-clustering bias in phase-amplitude cross-frequency coupling and its removal. *J. Neurosci. Methods* **254**, 60–72 (2015).
102. Mölle, M., Marshall, L., Gais, S. & Born, J. Grouping of spindle activity during slow oscillations in human non-rapid eye movement sleep. *J. Neurosci.* **22**, 10941–10947 (2002).

Acknowledgements

This work was supported by the STI 2030—Major Projects 2021ZD0200500, the National Natural Science Foundation of China (https://www.nsfc.gov.cn/, grant numbers 82072000 and 81671769), the Natural Science Foundation of Heilongjiang Province, China (http://kjt.hlj.gov.cn/, grant number YQ2023H016), the Fundamental Research Funds for the Central Universities (Grant No. HIT.OCEF.2023015).

Author contributions

Conceptualization by X.L., G.L. and Z.L.; data curation by C.T., J.W.; methodology by Z.L. and P.W.; software by and P.W.; writing draft by Z.L. and X.L.; validation by P.W.; investigation by Z.L., M.N., P.R., S.L., Q.L., L.S., K.L., W.D. and H.B.; supervision by X.L., G.L., L.Y. and L.Y.

Competing interests

The authors declare no competing interests.

Additional information

Supplementary information The online version contains supplementary material available at https://doi.org/10.1038/s42003-024-06941-9.

Correspondence and requests for materials should be addressed to Meng Na, Guoming Luan or Xia Liang.

Peer review information *Communications Biology* thanks Gregor Rainer and the other, anonymous, reviewer for their contribution to the peer review of this work. Primary Handling Editor: Benjamin Bessieres. A peer review file is available.